Rate and Distortion Optimization for Reversible Data Hiding Using Multiple Histogram Shifting

Junxiang Wang, Jiangqun Ni, *Member, IEEE,* Xing Zhang, Yun Qing Shi, *Fellow, IEEE*

***Abstract*—Histogram-shifting (HS) embedding as a typical reversible data hiding scheme is widely investigated due to its high quality of stego-image. For HS based embedding, the selected side information, i.e., peak and zero bins, usually greatly affects the rate and distortion performance of the stego-image. Due to the massive solution space and burden in distortion computation, conventional HS based schemes utilize some empirical criterion to determine those side information, which generally could not lead to a globally optimal solution for reversible embedding. In this paper, based on the developed rate and distortion model, the problem of HS based multiple embedding is formulated as the one of rate and distortion optimization. Two key propositions are then derived to facilitate the fast computation of distortion due to multiple shifting and narrow down the solution space, respectively. Finally, an evolutionary optimization algorithm, i.e., genetic algorithm (GA) is employed to search the nearly optimal zero and peak bins. For a given data payload, the proposed scheme could not only adaptively determine the proper number of peak and zero bin pairs but also their corresponding values for HS based multiple reversible embedding. Compared with previous approaches, experimental results demonstrate the superiority of the proposed scheme in the terms of embedding capacity and stego-image quality.**

***Index Terms*—Reversible data hiding, histogram shifting (HS), rate and distortion optimization, genetic algorithm (GA).**

I. Introduction

In recent years, data hiding techniques have found wide applications in copyright protection and content authentication of digital multimedia[1, 2]. The inherent defect of the conventional data hiding schemes is that they can usually not completely recover the original image after the image has been modified for data hiding. For some specific scenarios, such as military, medical and legal applications, even the slight distortion in images is not tolerated. Therefore, reversible data hiding techniques are developed, which enable the decoder to not only extract the secret data as traditional schemes, but also perfectly reconstruct the original cover image without any distortion.

Many reversible data hiding schemes have been reported in literature since Barton proposed his first reversible data hiding scheme [3] in 1997. In general, the existing reversible data hiding schemes explore the correlation among pixels in a cover image and can be mainly classified into three categories: i.e., lossless compression [4, 5], difference expansion (DE) [6–12] and histogram shifting (HS) [13–23]. DE based scheme was first proposed by Tian *et al*. [6]. Later, several improved techniques for DE based embedding are put forward, which includes the prediction and sorting [7, 9], and location map reduction [8, 10]. Histogram shifting (HS) based reversible data hiding was initially proposed by Ni *et al*. [13] in 2006, which selected a pair of peak and zero bins in histogram and then shifted the bins between the two bins by 1 towards zero bin for reversible data embedding. In principle, DE can be regarded as a special case of HS with peak and zero bins selected from the center and tail of the histogram, respectively. Therefore, we concentrate on the HS based approach throughout the paper.

The rate and distortion performance of HS based reversible data hiding depends heavily on the sharpness of histogram and the way to determine the peak and zero bin pairs. To sharpen the histogram, integer digital wavelet transform coefficients [14], pixel differences [15, 16], prediction errors [9, 17, 18] and interpolation errors [19] have been successively employed to generate the carrier image (to distinguish the cover images, we use carrier images throughout the paper to refer to the ones into which data are directly embedded, e.g., prediction and interpolation errors of cover images, etc.) for HS based embedding and relatively high embedding capacity are obtained. Among them, by taking advantage of the four adjacent neighbors around current pixel, Sachnev *et al*.'s prediction model [9] gives the sharpest histogram of prediction errors. Recently, to further improve the embedding capacity of carrier image, the concepts of statistical quantity histogram [20] and two-dimensional difference-histogram [21] have also been introduced, and the later is shown to be very suitable for low payload reversible data hiding. In addition to the generation of carrier images and their histograms, the determination of peak and zero bins is also critical for HS based embedding. For the small payload, single pair of peak and zero bins is sufficient and the optimal solution could be obtained through brute-force search. When relatively large payload is required, however, multiple embedding scheme as mentioned in [16] should be

This work was supported in part by the National Natural Science Foundation of China under Grants 61379156 and 61402209, in part by the National Research Foundation for the Doctoral Program of Higher Education of China under Grant 20120171110037, in part by the Key Program of Natural Science Foundation of Guangdong under Grant S2012020011114, in part by Invention Patent and Industrialization Technology Demonstration Project of Jiangxi Province (20143BBM26113). (*Corresponding author: Jiangqun Ni*).

J.X. Wang is with the School of Information Science and Technology, Sun Yat-sen University, Guangdong, 510006, China, and is also with the School of Mechanical & Electronic Engineering, Jingdezhen Ceramic Institute, Jiangxi, China (e-mail: wjx851113851113@163.com).

J.Q. Ni is with the school of Information Science and Technology, Sun Yat-Sen University, Guangdong 510006, China and is also with the State Key Laboratory of Information Security (Institute of Information Engineering, Chinese Academy of Sciences, Beijing 100093) (e-mail: issjqni@mail.sysu.edu.cn).

X. Zhang is with the School of Information Science and Technology, Sun Yat-Sen University, Guangdong 510006, China (e-mail: zhangxingkof@hotmail.com).

Y.Q. Shi is with the Department of Electronics and Computer Engineering, New Jersey Institute of Technology, Newark, New Jersey, USA (e-mail:shi@njit.edu).

employed, which uses multiple pairs of different peak and zero bins from the histogram at a time, and performs multiple HS based embedding consecutively based on the resulting histogram. Generally, with given data payload and carrier image, the design of HS based multiple reversible embedding can be formulated as the optimization problem to find a set of optimal peak and zero bins while minimizing its distortion. To solve the optimization problem, however, several key issues as follows should be addressed: (1) To develop the rate and distortion model for HS based multiple embedding. (2) To fast evaluate the distortion for multiple embedding. Note that, during multiple embedding, only one pair of peak and zero bins is selected for each embedding level, consequently the other peak and zero bins in the following embedding levels may be inevitably affected and changed to other values. To evaluate the distortion, the actual multiple embedding should be performed, which is heavily dependent on the relative location of the multiple peak and zero bins in the histogram and quite cumbersome and time-consuming. (3) To efficiently solve the optimization problem, i.e., to determine the number of optimal peak and zero bin pairs and their corresponding values. Due to the massive solution space, conventional HS based schemes usually follow some empirical search paths to find the peak and zero bin pairs, which generally do not ensure globally optimal solution for multiple reversible embedding.

Ni *et al*. in [13] orderly selected the highest frequency bins and their closest zero frequency bins as the peak and zero bins for HS based embedding. Based on the assumption that one peak bin should be on the left of the corresponding zero bin, Yang *et al*.in [22] proposed a general model for the distortion estimation. Unfortunately, they did not provide an efficient solution to find the optimal peak and zero bins. Moreover, the assumption itself may not always be true for practical applications. Xuan *et al*. in [23] proposed another HS based scheme to find the appropriate peak and zero bin pairs, which aimed to minimizing the possible histogram modification for given data payload. They utilized a pair of beginning and end thresholds to determine the interval around zero for successive assignment of peak bins. Although considerable improvement in performance was obtained, their scheme could not always guarantee the optimal peak bins be selected from the pre-determined interval. In addition, the scheme in [23] implied the zero bins be located at the tail of the histogram, which may lead to relatively large distortion due to histogram shifting and further sacrifice the performance. To our best knowledge, no practical rate and distortion optimization scheme for HS based multiple embedding has been reported in literature due to the massive solution space and the burden of distortion computation.

This paper presents a systematic framework to design HS based multiple reversible data hiding system with nearly optimal rate and distortion performance, which is independent of carrier images. And the contributions of the paper are as follows. Firstly, we develop the rate and distortion model for HS based multiple embedding, then present *Proposition 1* for fast evaluation of the possible distortion due to HS based multiple embedding without actually implementing the embedding process. We further provide the *Proposition 2* to significantly simplify the process of distortion evaluation when different peak and zero bins are paired for given candidate peak and zero bin sets. It is noted that there is no explicit expression of the rate and distortion in terms of multiple pairs of peak and zero bins, consequently the conventional optimization algorithms, such as gradient descent method etc., are not appropriate for application. In addition, the massive solution space of peak and zero bins also prohibit the direct use of exhaustive search in the design of optimal HS based multiple embedding. In [24], the evolutionary optimization algorithm, i.e., genetic algorithm (GA) was utilized to design a robust steganographic scheme that can break the inspection of steganalytic tools. In this paper, however, we also employ the GA with powerful global search capability and fast convergence, to automatically search the nearly optimal peak and zero bin pairs for HS based multiple embedding. Finally, the rhombus prediction in [9] is also incorporated to generate the carrier image for efficient reversible data embedding.

The rest of the paper is organized as follows. The rate and distortion model for HS based multiple embedding and the associated fast algorithm for distortion computation are developed in Section II. The specific GA is then designed to solve the optimization problem in Section III. The proposed embedding and extraction schemes are described in Section IV, which are followed by the experimental results and analysis in Section V. Finally, the conclusions are summarized in Section VI.

II. THE RATE AND DISTORTION MODEL FOR HS BASED MULTIPLE EMBEDDING

In the section, the rate and distortion model and the associated algorithm for fast distortion computation are developed. Based on these, the HS based multiple embedding is then formulated as the rate and distortion optimization problem in terms of multiple peak and zero bin pairs.

A. The rate and distortion model for HS based embedding

Histogram shifting (HS) algorithm is usually implemented on the histogram of grayscale values or predictive errors of the pixels. The precise rhombus predictor developed in [9] is employed in our proposed scheme to generate a much shaper histogram for efficient HS based embedding, which will be illustrated in Section IV. In the section, we concentrate on the development of the rate and distortion model for HS based multiple embedding.

1) HS embedding with single pair of peak and zero bins:

Based on a histogram of predictive errors, HS is performed to hide secret data. Before HS embedding, a peak bin with non-zero frequency and a zero bin with zero frequency in the histogram should be determined and denoted as (P_1, Z_1). HS then shifts the histogram bins between P_1 and Z_1 towards Z_1 direction by one unit to create a vacant position near P_1. Finally, each predictive error is scanned to embed 1-bit message w when P_1 is encountered. Let $pe(r, s)$ and $pe'(r, s)$ represent an original predictive error and the corresponding

marked one at (r, s), respectively. As illustrated in Fig.1, when $P_1 < Z_1$, HS is performed by

$$pe'(r,s) = \begin{cases} pe(r,s)+1, & pe(r,s) \in [P_1+1, Z_1-1] \\ pe(r,s)+w, & pe(r,s) = P_1 \\ pe(r,s), & otherwise \end{cases}. \quad (1)$$

In the case of $P_1 > Z_1$, HS is similarly implemented.

For the histogram shifting process with (P_1, Z_1) as side information, the embedding payload (rate) is calculated as

$$Payload = h(P_1), \quad (2)$$

where $h(P)$ denotes the frequency of occurrence for value P in histogram.

For an 8-bit grayscale image, predictive errors are located in the range $[-255, 255]$. To compute the distortion due to histogram shifting, the shift of each shifted bin for single embedding denoted as $\Delta(i)$ should be evaluated. For the secret message $\mathbf{w} = \{w\}$ of length C, when $P_1 < Z_1$, the actual HS embedding can be well illustrated in Fig.1, where all the bins located in the range $[P_1+1, Z_1-1]$ are shifted towards positive infinity by 1. With the assumption that the '0' and '1' in the message $\mathbf{w}$ are equally distributed, only half of the peak bins P_1 are shifted by 1,we then have the average shift at peak bin P_1

$$\delta(P_1) = +\frac{1}{2} \quad P_1 < Z_1. \quad (3)$$

Therefore, when $P_1 < Z_1$, the shift for HS single embedding is

$$\Delta(i) = \begin{cases} \delta(P_1) & i = P_1 \\ 1 & i \in [P_1+1, Z_1-1] \\ 0 & otherwise \end{cases}. \quad (4\text{-}1)$$

Similarly, we have the shift evaluation for $P_1 > Z_1$

$$\Delta(i) = \begin{cases} -\delta(P_1) & i = P_1 \\ -1 & i \in [Z_1+1, P_1-1] \\ 0 & otherwise \end{cases}. \quad (4\text{-}2)$$

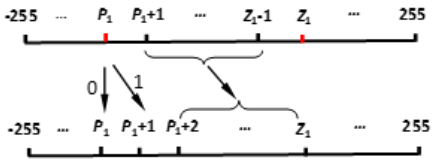

Fig. 1. The HS embedding process in the case of $P_1 < Z_1$

With the evaluated shift $\Delta(i)$, it is readily seen that the distortion D corresponding to the HS based single embedding as shown in Fig.1 can be computed as

$$D = \sum_{i \in [P_1, Z_1-1]} h(i) \times (\Delta(i))^2 = \sum_{i \in [P_1+1, Z_1-1]} h(i) + \frac{1}{2} \times C \ , \quad (5)$$

where $\sum h(i)$ and $\frac{1}{2} \times C$ in (5) denote the shifting distortion for bins in the range $[P_1+1, Z_1-1]$ and embedding distortion at peak bin P_1, respectively.

2) HS based multiple embedding:

When data payload is large, multiple embedding method is introduced, which utilizes several pairs of different peak and zero bins at a time and performs several levels of HS embedding consecutively based on the resulting histogram until all the selected peak and zero bin pairs are exhausted. For the several pairs of peak and zero bins involved in the HS based multiple embedding, each pair of peak and zero bins corresponds to one embedding level and affects one another, which should be taken into account and well tracked in distortion evaluation.

Fig.2 shows an example of HS based multiple embedding with two pairs of peak and zero bins. Firstly, two pairs of different peak and zero bins in the histogram are determined at a time and defined as $\{(P_k, Z_k) \,|\, k \in [1,2], P_1 \neq P_2 \text{ and } Z_1 \neq Z_2\}$.Then one pair of peak and zero bins, i.e., (P_1, Z_1), is chosen to perform the first level embedding, which makes P_2 shift to $P_2' = (P_2+1)$ in that P_2 locates in $[P_1+1, Z_1-1]$. Consequently, the peak bin for next embedding level should be replaced by $P_2' = (P_2+1)$ instead of P_2, which is referred to as "peak-bin drift" in our paper. Similarly we have "zero-bin drift". Based on (P_2', Z_2), the second level embedding is performed on the resulting histogram.

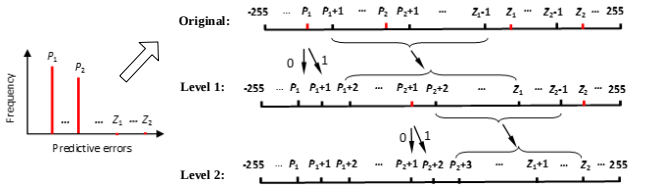

Fig. 2. An example of multiple embedding with two pairs of peak and zero bins

It is observed that each bin including the peak and zero in the histogram may experience several shifting for HS based multiple embedding, and the distortion introduced by each shifting should be processed separately through tracking the corresponding peak and zero bin "drift" caused by previous shifting. To compute the distortion with two-level embedding as shown in Fig.2 (the same for m-level embedding, $m > 2$), however, the accumulated shifts of each shifted bin should be evaluated, which is defined as

$$\mathbf{\Delta bin} = \{\Delta bin_i \mid i \in [-255, 255]\}, \quad (6)$$

where Δbin_i represents the accumulated shifts of the i^{th} bin.

By consecutively implementing two single HS embedding with (P_1, Z_1) and (P_2+1, Z_2), and taking into account of the bin shifts arising from each single HS embedding, we have

$$\Delta bin_i = \begin{cases} +\delta(P_1) & i = P_1 \\ +1 & i \in [P_1+1, P_2-1] \\ +1+\delta(P_2) & i = P_2 \\ +1+1 & i \in [P_2+1, Z_1-1] \\ +1 & i \in [Z_1+1, Z_2-1] \\ 0 & otherwise \end{cases}. \quad (7)$$

It is noted that, to compute the accumulated shifts of each bin, the "peak bin drift" for P_2 is required to be tracked and

its effects should be taken into account. Thus the distortion D caused by the two-level embedding process is computed by

$$\begin{aligned} D &= \sum_{i\in[-255,255]} h(i)\times(\Delta bin_i)^2 = \sum_{\substack{i\in[-255,255]\\ \Delta bin_i = Fix(\Delta bin_i)}} h(i)\times(\Delta bin_i)^2 + \sum_{\Delta bin_i \neq Fix(\Delta bin_i)} D_i \\ &= \sum_{\substack{i\in[-255,255]\\ i\notin\{P_1,P_2\}}} h(i)\times(\Delta bin_i)^2 + (D_{P_1}+D_{P_2}) \end{aligned}, \quad (8)$$

where $D_{P_k}(k=1,2)$ denotes the embedding distortion at the peak bin P_k and $Fix(\bullet)$ is the round function that rounds its inputs toward zero, e.g. $Fix(3.6)=3$ and $Fix(-3.6)=-3$. With $Fix(\bullet)$, it is easy to identify bin i as peak bin if the condition $\Delta bin_i \neq Fix(\Delta bin_i)$ is met (Note that accumulate shift in peak bin is not integer as shown in Equ.(7)). Without loss of generality, let $d=Fix(\Delta bin_i), (i=P_k)$ for the peak bin P_k, $D_{P_k}(k=1,2)$ can be individually computed by

$$D_{P_k}=\begin{cases} \frac{1}{2}\times h(P_i)\times(d)^2+\frac{1}{2}\times h(P_i)\times(d+1)^2, & \Delta bin_i > Fix(\Delta bin_i) \\ \frac{1}{2}\times h(P_i)\times(d)^2+\frac{1}{2}\times h(P_i)\times(d-1)^2, & \Delta bin_i < Fix(\Delta bin_i) \end{cases}, \quad (9)$$

where $k\in[1,2]$.

For a HS based multiple embedding with m pairs of peak and zero bins as side information, i.e., $\{(P_k,Z_k)\mid 1\le k\le m\}$, its embedding payload (rate) is

$$Payload=\sum_{i=1}^{m} h(P_i). \quad (10)$$

While the distortion for m-level multiple embedding can be evaluated based on its accumulated shift array $\mathbf{\Delta bin}$, i.e.,

$$\begin{aligned} D &= \sum_{i\in[-255,255]} h(i)\times(\Delta bin_i)^2 \\ &= \sum_{\substack{i\in[-255,255]\\ i\notin\{P_k\mid k\in[1,m]\}}} h(i)\times(\Delta bin_i)^2 + \sum_{k=1}^{m} D_{P_k}, \end{aligned} \quad (11)$$

where the distortion $D_{P_k}(k=1,2,\ldots,m)$ due to peak bin shift can be similarly obtained as (9).

According to aforementioned, to exactly evaluate the distortion for multiple embedding with fixed m pairs of peak and zero bins, the accumulated shifts for each bin, i.e., the shift array $\mathbf{\Delta bin}$ should be computed, which is cumbersome and time-consuming. The computation involves the tracking of both "peak-bin drift" and "zero-bin drift", dynamically updating the peak and zero bins for each embedding level and the actual implementation of m-level multiple shifting. A close observation of the two-level embedding process as shown in Fig.2, however, suggests that the accumulated shifts of each bin for HS based multiple embedding looks like to be obtained in a "de-coupled" way. *Proposition 1* in next subsection will be put forward to confirm the conjecture and the associated fast algorithm will then be developed in next subsection to compute the distortion for HS based multiple embedding. For given m peak and zero bins, another important issue in rate and distortion optimization is the evaluation of distortion when different peak and zero bins are paired and sequentially arranged in the process of multiple embedding. The problem is highly challenging since the inherent combinatorial nature often bears prohibitive computational complexity and renders the problem intractable. And *Proposition 2* will also be proposed to tackle the issue for rate and distortion optimization of HS based multiple embedding.

B. Main results of fast distortion computation for HS based multiple embedding

In this subsection, two propositions and the associated algorithms are presented to cope with the issues of fast distortion computation for HS based multiple embedding with fixed m pairs of peak and zero bins, and the fast distortion evaluation when different peak and zero bins are paired and sequentially arranged for given m peak and zero bins, respectively.

Proposition 1. For a HS based multiple embedding with histogram H, and fixed m pairs of peak and zero bins as side information, denoted as $\{(P_k,Z_k)|1\le k\le m\}$,$P_i\neq P_j$,$Z_i\neq Z_j$, $i\neq j$ and $i,j\in[1,m]$, the accumulated shifts Δbin_i for bin i after m-level embedding are equivalent to the sum of m independent shift $\Delta_k(i)$ due to HS single embedding with initial histogram H and (P_k,Z_k), i.e., $\Delta bin_i=\sum_{k=1}^{m}\Delta_k(i)$, where $\Delta_k(i)$ denotes the shift of the k^{th}-level embedding with (P_k,Z_k) and is calculated with (4-1) or (4-2). ■

In the interest of focused presentation, the strict mathematical proof for *Proposition 1* is included in the supplementary file (available at http://ieeexplore.ieee.org). Based on that, a fast algorithm can be developed to evaluate the accumulated shifts of each bin for HS based multiple embedding. Instead of actually performing the multiple embedding and dynamically tracking the "peak-bin drift" and "zero-bin drift", our approach only involves the computation of the bin shift for m independent HS single embedding with the same initial histogram H using (4-1) or (4-2), and finally adds the shifts together to obtain the accumulated shifts. With the accumulated shifts, the overall distortion is then obtained using (11).

We then proceed to investigate the distortion computation for HS based multiple embedding with given m peak and zero bins when different peak and zero bins are paired and sequentially arranged, which is effectively resolved with *Proposition 2* below.

Proposition 2. Let $\mathbf{P}$=$\{P_1,P_2,\ldots,P_m\}$ and $\mathbf{Z}$=$\{Z_1,Z_2,\ldots,Z_m\}$, $P_i\neq P_j$,$Z_i\neq Z_j$,$i\neq j$ and $i,j\in[1,m]$, be the given m peak and zero bins. For HS based multiple embedding with m pairs of peak and zero bins, different permutation of $\mathbf{P}$ and $\mathbf{Z}$ leads to an identical distortion. ■

Note that the $\mathbf{P}$ and $\mathbf{Z}$ above are ordered sets with their elements in the set from left to right indicating the sequential order in the implementation of HS based multiple embedding. With *Proposition 2*, the computational complexity of distortion evaluation for the HS based multiple embedding with given m peak and zero bins is substantially decreased by $A_m^m\times A_m^m$, where A_n^k is the number of k permutations of n. Therefore, the solution space is significantly reduced accordingly. *Proposition 2* itself can also be strictly proved using mathematical induction. Since it is rather technical, the details are presented in the supplementary file (available at http://ieeexplore.ieee.org).

C. Rate and distortion optimization

On the basis of the developed rate and distortion model for HS based multiple embedding, we have the rate and distortion optimization for payload-limited embedding. Before formulating the optimization problem, the range for the tunable parameters, i.e., P_k, Z_k, and m, should be defined. Let the number of peak and zero bin pairs m in the predefined range $[1, M_{max}]$. For the histogram of a carrier image (prediction errors) with bins located in the range $[-255, 255]$, all the bins with zero frequency are candidates for zero bins, i.e., $\mathbf{Zero\_Set} = \{Z_k \mid k \in [1, l]\}$, where l denotes the number of the candidate zero bins in the histogram. While other bins except zero ones are considered as the candidates for peak bins and denoted as $\mathbf{Peak\_Set} = \{P_k \mid k \in [1, 511 - l]\}$.

Payload-limited embedding. In practice, the HS based multiple reversible data hiding can usually be formulated as the payload-limited embedding, i.e.,

$$\begin{cases} \min\limits_{\{(P_k, Z_k), m | k \in [1,m]\}} D[(P_k, Z_k)_{k=1,\ldots,m}] \\ P_k \in \mathbf{Peak\_Set}, Z_k \in \mathbf{Zero\_Set}, m \in [1, M_{max}] \\ s.t. \sum\limits_{k=1}^{m} h(P_k) \geq C \\ P_i \neq P_j, Z_i \neq Z_j, i \neq j \text{ and } i, j \in [1, m] \end{cases}, \quad (12)$$

where D is the distortion calculated with the *Proposition 1* (for accumulated shifts) and distortion model (11). The rate and distortion optimization problem in (12) is to determine the number of peak and zero bin pairs m among the predefined range $[1, M_{max}]$ and the corresponding values of peak and zero bins $\{(P_k, Z_k) | k \in [1, m]\}$ from **Peak_Set** and **Zero_Set** that embeds a given payload C while minimizing the distortion D. Therefore, if m is fixed, the size of solution space for (12) is $A_l^m \times A_{511-l}^m$. Take the predictive errors of Lena image as example, where $l = 92$, the size of solution space is approximately $A_{92}^{10} \times A_{511-92}^{10} = 3.0466 \times 10^{32}$ in the case of $m = 10$. In addition, to optimize the rate and distortion performance, it is desirable to try all the possible pair number m among the range ($m \in [1, M_{max}]$) and thus the size of total solution space is $\sum_{m=1}^{M_{max}} A_l^m \times A_{511-l}^m$. On the other hand, the combinatorial nature of the problem also makes the conventional approaches, such as gradient based or numerical search methods, fail to achieve good results. Therefore, the evolutionary optimization algorithm, such as genetic algorithm (GA), is adopted to solve the rate and distortion optimization problem in (12) in next section. It is worth noting that, although other evolutionary algorithms, such as particle swarm optimization (PSO), could also be utilized, our simulation results indicate that both GA and PSO have comparable rate and distortion performance for HS based multiple reversible embedding. If a specific optimal (or sub-optimal) solution with given m pairs of peak and zero bins exists, then according to *Proposition 2* and (10), different combinations between these peak and zero bins lead to the same rate and distortion performance. Therefore, the chance to find an optimal solution is substantially increased for GA, or equivalently the solution space size is reduced dramatically to $\sum_{m=1}^{M_{max}} C_l^m \times C_{511-l}^m$ (C_n^k is the number of k combinations of n), which is more preferable for practical application of GA. By taking advantage of fast convergence and powerful global search ability of GA, we could not only adaptively determine the nearly optimal number of peak and zero bin pairs but also their corresponding values for a given payload.

III. RATE AND DISTORTION OPTIMIZATION USING GENETIC ALGORITHM

A. The framework of the proposed genetic algorithm

Aiming to optimize the rate and distortion performance described in (12), we design a genetic algorithm (GA) to automatically determine the tunable parameters, i.e., the number of peak and zero bin pairs m and their corresponding values. During the GA process, the two constraints on payload and assignment of peak and zero bins as shown in (12) should be specially considered.

Our genetic algorithm follows the framework of conventional genetic methodology as described in [25], which includes several problem oriented designs. Starting with an initial randomly generated pool of population, into which some specifically designed empirical chromosomes with good genes are added to ensure better convergence for GA implementation. Let g, G_{max}, N and M_{max} denote the current generation number, the maximum generation number, the amount of individuals in the initial population and the predefined upper bound of peak and zero bin number m, respectively. The overall structure of the proposed genetic algorithm includes: 1) initialization; 2) empirical chromosomes addition; 3) evaluation of the population; 4) parents' selection for reproduction; 5) crossover and mutation; and 6) selection for next generation construction, which is well illustrated in Fig.3. In the next subsection, we will describe some problem oriented designs for our GA scheme different from the conventional ones.

B. Chromosome encoding

To solve the rate and distortion optimization problem described in (12) using GA, all the tunable parameters, i.e., the number of peak and zero bin pairs and the corresponding values of peak and zero bins should be represented with chromosome encoding. The chromosome vector consists of $3M_{max}$ elements (genes) and is defined as:

$$\begin{aligned} \mathbf{C}^t &= (\mathbf{I}^t, \mathbf{P}^t, \mathbf{Z}^t) \\ \mathbf{I}^t &= \{i_k \mid i_k \in \{0, 1\} \text{ and } k \in [1, M_{max}]\} \\ \mathbf{P}^t &= \{P_k \mid P_k \in \mathbf{Peak\_Set} \text{ and } k \in [1, M_{max}]\} \\ \mathbf{Z}^t &= \{Z_k \mid Z_k \in \mathbf{Zero\_Set} \text{ and } k \in [1, M_{max}]\} \end{aligned}, \quad (13)$$

where $\mathbf{C}^t$ refers to the t^{th} individual chromosome in a population. It is actually a composite chromosome consisting of three different types of chromosomes. The first section of $\mathbf{C}^t$, i.e., $\mathbf{I}^t$ is designed for indicating bits, while $\mathbf{P}^t$ and $\mathbf{Z}^t$ each includes at most M_{max} different peak and zero bins chosen from the **Peak_Set** and **Zero_Set** , respectively.

The element i_k ='1' in $\mathbf{I}^t$ indicates that k^{th} pair of peak and zero bins (P_k, Z_k) from $\mathbf{P}^t$ and $\mathbf{Z}^t$ would be activated for HS based multiple embedding, otherwise, the pair (P_k, Z_k) is ignored. With the adoption of indication bits $\mathbf{I}^t$ in the chromosome, the number of involved peak and zero bin pairs for multiple embedding could be dynamically adjusted in the range $[1, M_{max}]$.

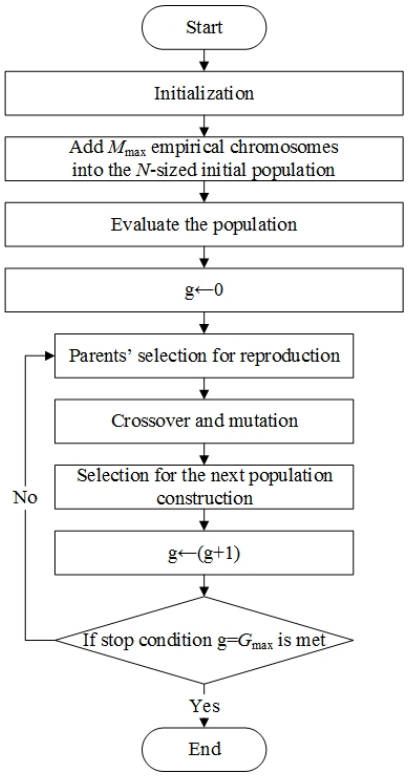

Fig. 3. Flowchart of the proposed GA scheme

C. Empirical chromosomes addition

We then proceed to investigate the way to improve the capability of the proposed GA to find the nearly optimal solution by introducing some empirical chromosomes with good genes. When the payload C is large, the constraint $\sum_{i=1}^{m} h(P_i) \geq C$ specifies a relatively tiny feasible solution space compared with the entire solution space $\sum_{m=1}^{M_{max}} C_l^m \times C_{511-l}^m$, it is usually difficult to find even the feasible solution, let alone the optimal one based on the randomly selected initial chromosomes through limited generations of evolution with GA. Let F_C denote the feasible solution space size corresponding to the constraint $\sum_{i=1}^{m} h(P_i) \geq C$, the probability of reaching the feasible solutions by randomly selected initial chromosomes is

$$prob = \frac{F\_C}{\sum_{m=1}^{M_{max}} C_l^m \times C_{511-l}^m}, \tag{14}$$

where the denominator $\sum_{m=1}^{M_{max}} C_l^m \times C_{511-l}^m$ is the size of the entire solution space as mentioned in Section II-C. According to our experiments, it is usually difficult for GA to find the feasible solutions within finite generations of evolution with randomly selected initial chromosomes when the payload is relative large, e.g., $C \geq 2 \times 10^5$ bits for cover image Lena of $512 \times 512 \times 8$ bit.

To solve the problem, we manually construct a group of empirical individuals (chromosomes), which include the peak and zero bins determined using some existing criterion [13] and are adopted in the initial population. In our implementation, at most M_{max} empirical individuals are introduced, where the chromosome $\mathbf{C}^t, t \in [1, M_{max}]$ includes t different peak bins with highest frequency from **Peak_Set** and t different zero bins closest to the corresponding peak bins from **Zero_Set**, respectively.

The adoption of empirical chromosomes shows some advantages. One is that, rather than a completely random search, these chromosomes indicate the search direction towards the feasible solutions space (i.e.,$\sum_{i=1}^{m} h(P_i) \geq C$) and ensure stable convergence for GA when the payload is large. Next, the evolution mechanism of GA generally guarantees to achieve a better performance than the ones with the empirical peak and zero bins in the initial population.

D. Fitness Evaluation

The objective of the proposed GA process is to find the nearly optimal solution in terms of multiple pairs of peak and zero bins associated with the minimal distortion D. The involved selection scheme, such as roulette wheel selection, however, tends to choose the chromosome with higher fitness value. Thus the distortion D itself cannot be taken directly as the fitness value. Let D_{max} be the possible maximal distortion for the given HS based multiple embedding in one generation, a proper fitness value can be defined as follows

$$fitness = D_{max} - D \ . \tag{15}$$

In addition, to ensure the feasible output satisfying the payload constraint $\sum_{i=1}^{m} h(P_i) \geq C$ in (12), the penalty with predefined large value, say 10^7, is assigned to the distortion D of the infeasible chromosomes, which makes them be eliminated with high probability during the selection process.

IV. EMBEDDING AND EXTRACTION PROCESSES

In general, our GA based rate and distortion optimization scheme is independent of the carrier images, either in pixel or prediction domain. The accurate rhombus prediction proposed in [9] is incorporated in our work to generate the prediction errors with much shaper histogram which would lead to significant performance improvement for HS based multiple embedding. To perform rhombus prediction, the pixels in an image are divided into two sets, i.e., the Cross set (X) and the Round set (O) as shown in Fig.4(a). Hereinafter, we denote the pixels and prediction errors in these two sets as P_Z and PE_Z(Z = 'X' or 'O'), respectively. Each pixel in Cross set is predicted with its four neighboring pixels in Dot set as shown in Fig.4(b) and vice versa.

$$\hat{P}_X(i,j) = round\left[\frac{P_O(i-1,j)+P_O(i+1,j)+P_O(i,j-1)+P_O(i,j+1)}{4}\right], \tag{16}$$

where $round(\bullet)$ is the function that returns the nearest integer of the input. The corresponding prediction error $PE_X(i,j)$ is computed as follows

$$PE_X(i,j) = P_X(i,j) - \hat{P}_X(i,j) \ . \tag{17}$$

As the performance of the proposed GA scheme depends heavily on the carrier image, we also sort the prediction errors in their local variances ascending order [9] and take the top $\chi(\%)$ of the prediction errors for HS based multiple embedding. According to our experiments, the optimum $\chi(\%)$ is in the collections $\Lambda_1 = \{10, 20, 30, 40, 50\}$ for low data

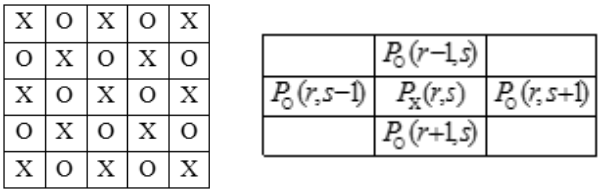

(a) (b)

Fig. 4. The sketch of rhombus prediction

payload (< 0.1 bpp) and $\Lambda_2 = \{50, 60, 70, 80, 90, 100\}$ for medium to high payload applications (≥ 0.1 bpp), respectively.

A. Embedding Process

For a 8-bit grayscale cover image and the binary secret message $\mathbf{w}$ of length C, the embedding process is described briefly as follows.

1) **Initialization**. With the cover image in Cross and Round sets as shown in Fig.4(a), assign half of the secret message of length $1/2 \times C$ for Cross and Round sets embedding, respectively.
2) **Rhombus prediction of the Cross set**. As shown in Fig.4(b), each pixel in the Cross set is predicted by its four neighboring pixels in Round set to obtain the $\hat{P}_X(r,s)$ and then the prediction error $PE_X(r,s)$ in the Cross set.
3) **Optimal peak and zero bins selection**. Based on the histogram of prediction errors in the Cross set, i.e., $PE_X = \{PE_X(r,s)\}$, the GA based rate and distortion optimization is carried out to determine the nearly optimal number of peak and zero bin pairs and their corresponding values for the payload of length $\frac{1}{2}C$.
4) **Cross set embedding**. To hide the message into the prediction errors PE_X, the accumulated shifts $\mathbf{\Delta bin} = \{\Delta bin_i\}$ for each bin after the multiple embedding are calculated by application of *Proposition 1* to generate the marked prediction errors in Cross set. Let $PE_X(r,s) = i$, we have

$$PE'_X(r,s)=\begin{cases} PE_X(r,s)+\Delta bin_i, & \Delta bin_i=Fix(\Delta bin_i) \\ PE_X(r,s)+Fix(\Delta bin_i)+w, & \Delta bin_i>Fix(\Delta bin_i), \\ PE_X(r,s)+Fix(\Delta bin_i)-w, & \Delta bin_i<Fix(\Delta bin_i) \end{cases} \tag{18}$$

where w denotes 1-bit secret data, Δbin_i is the accumulated shifts of bin i.
5) **Stego-pixels generation in the Cross set**. With marked prediction errors, we have the stego-pixels in the cross set

$$P'_X(r,s) = PE'_X(r,s) + \hat{P}_X(r,s) \ . \tag{19}$$

6) **Stego-pixels generation in the Round set**. Utilize the generated stego-pixels in the Cross set to predict the pixels in Round set as mentioned in Step 2 and repeat Step 3-5 to generate the stego-pixels $P'_O(r,s)$ in the Round set.
7) **Stego image generation**. Combine the stego-pixels in both Cross and Round sets, i.e., P'_X and P'_O to obtain the whole stego-image.

Note that, the above GA based multiple embedding should be tested for the possible χ in $\Lambda(\Lambda_1$ or $\Lambda_2)$ to determine the optimum χ_{opt} in terms of rate and distortion performance. For a given payload, we take the same percentage χ in both Cross and Round sets to simplify the implementation. Besides, the Luo's method [19] is also employed in the embedding process to avoid the possible overflow/underflow for the generated stego image, in which, a location map is introduced to indicate the overflowed/underflowed pixels and then hidden in the carrier images as the additional side information.

B. Extraction Process

Based on the received optimal χ_{opt}, peak and zero bins and the stego-image, we extract the secret message and recover the original image in the inverse order as embedding process, namely the marked Round set is recovered and message is extracted first, which is then used to reconstruct the marked Cross set and extract the corresponding hidden message.

V. EXPERIMENTAL RESULTS AND ANALYSIS

To evaluate the proposed rate and distortion optimization scheme, we test several $512 \times 512 \times 8$ bits grayscale images with different texture characteristics from SIPI database [26] and 100 $512 \times 512 \times 8$ bits grayscale images randomly selected from Bossbase ver.1.01 [27]. By comparing the proposed scheme with some state-of-the-art reversible data hiding methods, the superiority of our scheme is verified.

A. Parameters' setting and empirical chromosomes addition for Genetic Algorithm

Before comparing it to prior works, we first discuss the parameters' setting of our GA based multiple embedding scheme. To simplify the analysis, we set most of the GA parameters experimentally, e.g., population size, crossover rate, mutation rate, maximum pair number M_{max} and the maximum generation number G_{max}, as shown in Table I. In addition, the effectiveness of empirical chromosomes addition is also investigated.

TABLE I
PARAMETERS' SETTING OF THE PROPOSED GENETIC ALGORITHM

Parameters	Values
Population size N	100
Maximal pair number M_{max}	20
Mutation rate m_rate	0.1
Crossover rate c_rate	0.8
Maximum generation number G_{max}	100

For a small payload of $C/2 = 10^4$ bits (i.e., 0.076 bits/pixel) embedded in the Cross set of Lena, Fig.5 gives the convergence results when initial empirical chromosomes (good seeds) are not included /and included, respectively. The $M_{max} = 20$ pairs of different peak and zero bins described

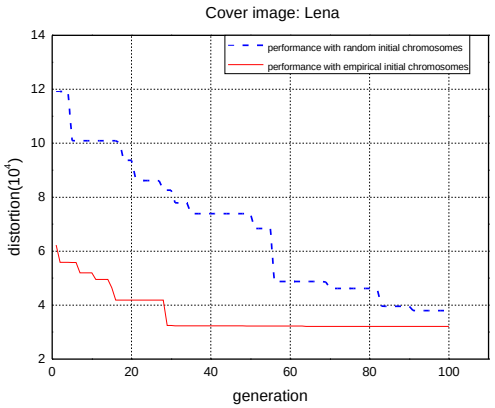

Fig. 5. The distortion versus the number of generation for test image Lena at small payload (0.076 bits/pixel)

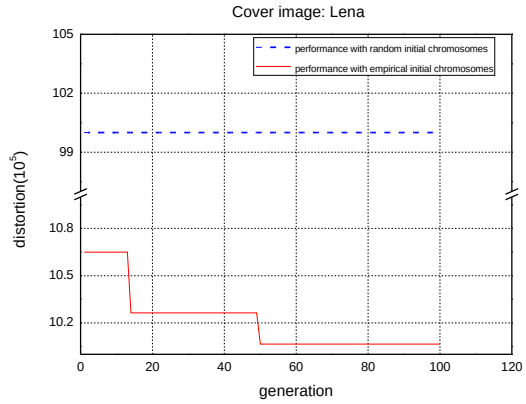

Fig. 6. The distortion versus the number of generation for test image Lena at large payload (0.763 bits/pixel)

in III.C [13] are utilized as the initial "good" chromosomes in our implementation. It is observed that, whether the initial empirical chromosomes are included or not, the GA based multiple embedding scheme converges within a rather limited generations of evolution. The adoption of some initial "good" seeds, however, would speed up considerably the convergence and achieve a better performance in terms of distortion. This is because, compared with the randomly selected seeds (chromosomes), the introduction of those "good" seeds into the initial population can provide better genes for evolution and thus a better solution is easier to be reached with higher probability. For a large payload, say $C/2 \geq 10^5$(i.e., 0.763 bits/pixel), however, the implementation of the proposed scheme is heavily dependent on the help of some initial "good" seeds. The payload constraint itself, i.e., $\sum_{i=1}^{m} h(P_i) \geq C$, makes it difficult for the GA based scheme to find a payload feasible solution based on the randomly selected initial seeds within limited generations of evolution. Fig.6 includes the corresponding convergence performance, where the distortions are consistently around the predefined penalty value, i.e., 10^7, even after 100 generations of evolution. In contrast, the addition of specifically designed seeds in the initial population can not only meet the payload constraint but also quickly reach the nearly optimal solution and ensure the stable convergence as shown in Fig.6. Therefore, the effectiveness of empirical chromosomes addition is verified. In addition, according to our experimental results, the maximum generation number $G_{max}=70$ is sufficient to obtain the stable convergence for medium textured images, such as Lena. While G_{max} is a little bit larger in the range $[70, 100]$ for other highly textured images, such as Baboon, owing to the slower convergence speed.

B. Comparison with other related schemes

We first compare our GA based multiple embedding scheme with three typical methods (Ni *et al*. [13], Xuan *et al*. [23] and Sachnev *et al*. [9]) in terms of peak and zero bins selection for various payloads. In the interest of fair comparison, our scheme (with $\chi(\%) \in \Lambda_1 \cup \Lambda_2$) and other related methods are implemented on the same Cross set of test images with rhombus prediction. Table II summarizes the rate (payload) and distortion performance of the involved schemes and the corresponding values of peak and zero bins for image Lena.

It is noted that the distortion performance of our scheme in Table II is the average over 10 experiments for each payload and represents in the form "Mean $\pm$ Standard Deviation". While the listed peak and zero bins of our scheme correspond to the solution whose distortion is closest to the average one for each payload.

It is demonstrated in Table II that our GA based scheme achieves the best rate and distortion performance for various data payloads. Compared with the proposed scheme, both the methods in [13] and [9] determine the peak bins based on some empirical rules. Ni *et al*. [13] uses in priority the peak bins with higher frequency, while the DE method in [9] is actually a special case of HS with the peak bins fixedly selected from an interval $[T_n, 0] \cup [0, T_p]$, ($T_n < 0$ and $T_p \geq 0$) around zero, where T_n and T_p are pre-defined thresholds. Although the method in [23] shows some adaptability in peak bin selection, the employed peak bins are also confined and successively assigned from an interval determined. Moreover, the peak bins employed in [9], [13] and [23] are generally located around 0 and the zero bins in [9] and [23] are selected from the tail of histogram, therefore the corresponding shifting distortion is further increased.

According to our understanding, the good rate and distortion performance of our GA based multiple embedding can be achieved in two aspects. For one thing, instead of utilizing one or two high frequency bins as peak bins which corresponds to high shifting distortions, several relatively low frequency bins may be a better choice in the case of small data payload. For another, those two peak and zero bin pairs should be determined in priority, i.e.: (1) their associated shiftings are in the reverse direction with each other; (2) their associated shiftings share as much overlapped bins with high frequency as possible. For this example, the (P_1, Z_1) and (P_2, Z_2) as shown in Fig.7 are two peak and zero bin pairs shifting in reverse direction. According to *Proposition 1* in Section II-B, the accumulated shifts in the overlapped bins between $[P_1, P_2]$ can be eliminated, which gives rise to reduced shifting distortions. It is also observed in Table II that, for low data payload (0.076bpp), rather than the high frequency bin 0, our scheme selects two low frequency bins 3 and -3 as the peak

TABLE II
THE SELECTED PEAK AND ZERO BINS FOR INVOLVED SCHEMES IN THE CROSS SET OF IMAGE LENA WITH $512 \times 512 \times 8$ BITS

Payload in bits (bpp)	Schemes	Selected peak and zero bins (P,Z)	Distortion
10,000 (0.076bpp)	Our scheme ($\chi = 60\%$)	$(3,-136),(-3,23)$	$1.941 \times 10^4 \pm 3.56 \times 10^2$
	Scheme [13]	$(0,42)$	6.230×10^4
	Scheme [23]	$(2,56)$	3.215×10^4
	Scheme [9]	$(0,32)$	2.687×10^4
30,000 (0.23 bpp)	Our scheme ($\chi = 80\%$)	$(1,-29),(-1,36),(6,81)$	$8.3661 \times 10^4 \pm 2.1 \times 10^3$
	Scheme [13]	$(-1,-43),(0,42)$	1.131×10^5
	Scheme [23]	$(-1,-45),(1,56)$	9.651×10^4
	Scheme [9]	$(-1,-28),(0,38)$	8.477×10^4
60,000 (0.458bpp)	Our scheme ($\chi = 80\%$)	$(0,-29),(-1,-31),(1,-74),(-2,30),(-5,102),(8,-42)$ $(-16,190),(16,249)$	$3.0665 \times 10^5 \pm 1.14 \times 10^3$
	Scheme [13]	$(-2,-45),(-1,-43),(0,42),(1,46)$	3.587×10^5
	Scheme [23]	$(-2,-46),(-1,-45),(0,56),(1,57)$	3.587×10^5
	Scheme [9]	$(-2,-35),(-1,-34),(0,41),(1,42)$	3.095×10^5
100,000 (0.763bpp)	Our scheme ($\chi = 90\%$)	$(-5,206),(5,-38),(-4,-29),(-3,48),(3,-32),(2,39),(-2,-44)$ $(1,190),(-1,-45),(0,51),(-17,-141),(-16,-69),(19,225)$	$9.038 \times 10^5 \pm 1.54 \times 10^3$
	Scheme [13]	$(-4,-47),(-3,-46),(-2,-45),(-1,-43),(0,42),(1,46),(2,47)$ $(3,48),(4,49)$	1.0648×10^6
	Scheme [23]	$(-4,-45),(-3,-46),(-2,-47),(-1,-48),(0,56),(1,57),(2,58)$ $(3,59),(4,60)$	1.0649×10^6
	Scheme [9]	$(-4,-44),(-3,-43),(-2,-42),(-1,-41),(0,41),(1,42),(2,43)$ $(3,44),(4,45)$	9.314×10^5

bins and the bin shifts in reverse direction between $[-3,3]$ would offset each other. As the prediction errors of natural images are Laplacian distributed, and the highest frequency bins are located close to bin 0, the shifting distortions are thus significantly reduced. The same happened to the medium payload embedding (0.23bpp and 0.458bpp in Table II). Note that, for the case of 0.076bpp and 0.23bpp, although the peak and zero bins in (-3,-136)[1] and (6,81) are far apart from each other, the bins in between each of these two peak and zero bin pairs are sparse and have low frequency, which corresponds to much less shifting distortions.

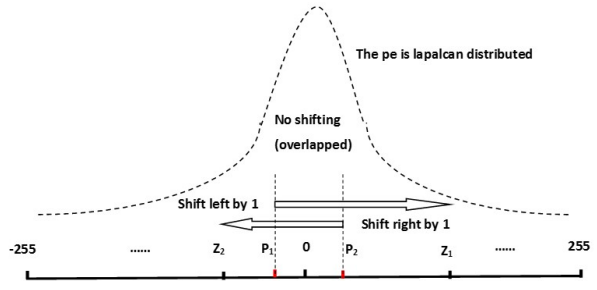

Fig. 7. The illustration of bin shift cancellation

We then proceed to compare the comprehensive performance between our scheme and some state-of-the-art reversible data hiding methods, which include two DE based methods in predictive errors (Sachnev *et al*. [9] and Li *et al*.[12]), three HS based methods (Wu *et al*. [18], Luo *et al*. [19] and Xuan *et al*. [23]). In our implementation of the GA based embedding scheme, both the Cross and Round sets of cover images are utilized with rhombus prediction and sorting to ensure the better rate and distortion performance (refer to section IV-A). Note that the embedding payload is the effective one except the location (boundary) map and multiple peak and zero bins. For small to medium data payload, i.e., ER(Embedding Rate)≤ 0.4 bpp, which is ideal for HS based multiple embedding and most commonly used in practical applications, our scheme achieves the best rate and distortion performance among all the methods, for the test images Lena, Baboon, F16 and Peppers as shown in Fig.8. The same happened to the average performance comparison with 100 test images randomly selected from image database BOSSbase ver. 1.01 [27], as illustrated in Fig.9. It is observed that, for large data payload (ER$>$0.4 bpp), although our scheme outperforms consistently the other three HS based methods [18, 23, 25], its performance tends to be similar to Sachnev *et al*.'s method [9]. This is because the proposed scheme and the method in [9] are all implemented on the errors of rhombus prediction. At high embedding rate, the important bins with high frequency in the histogram should be utilized by all the involved schemes to hide large payload. Under these circumstances, our scheme could not exemplify its advantage in peak and zero bin selection. It is also observed that the proposed scheme cannot compete Li *et al*'s method [12] for Pepper image at high data payload. This is because the Pepper image has many potentially overflowed/underflowed pixels located around both sides of the histogram, i.e. 0 and 255. Instead of embedding only 1 bit at a pixel with our scheme, Li *et al*'s method could choose the appropriate smooth areas in images to hide more than 1 bit data at a pixel, thus Li *et al*'s method may utilize much less potentially overflowed/underflowed pixels

[1]The original peak and zero bin pair is (3,-136), and the shifts in [-3,3] are canceled.

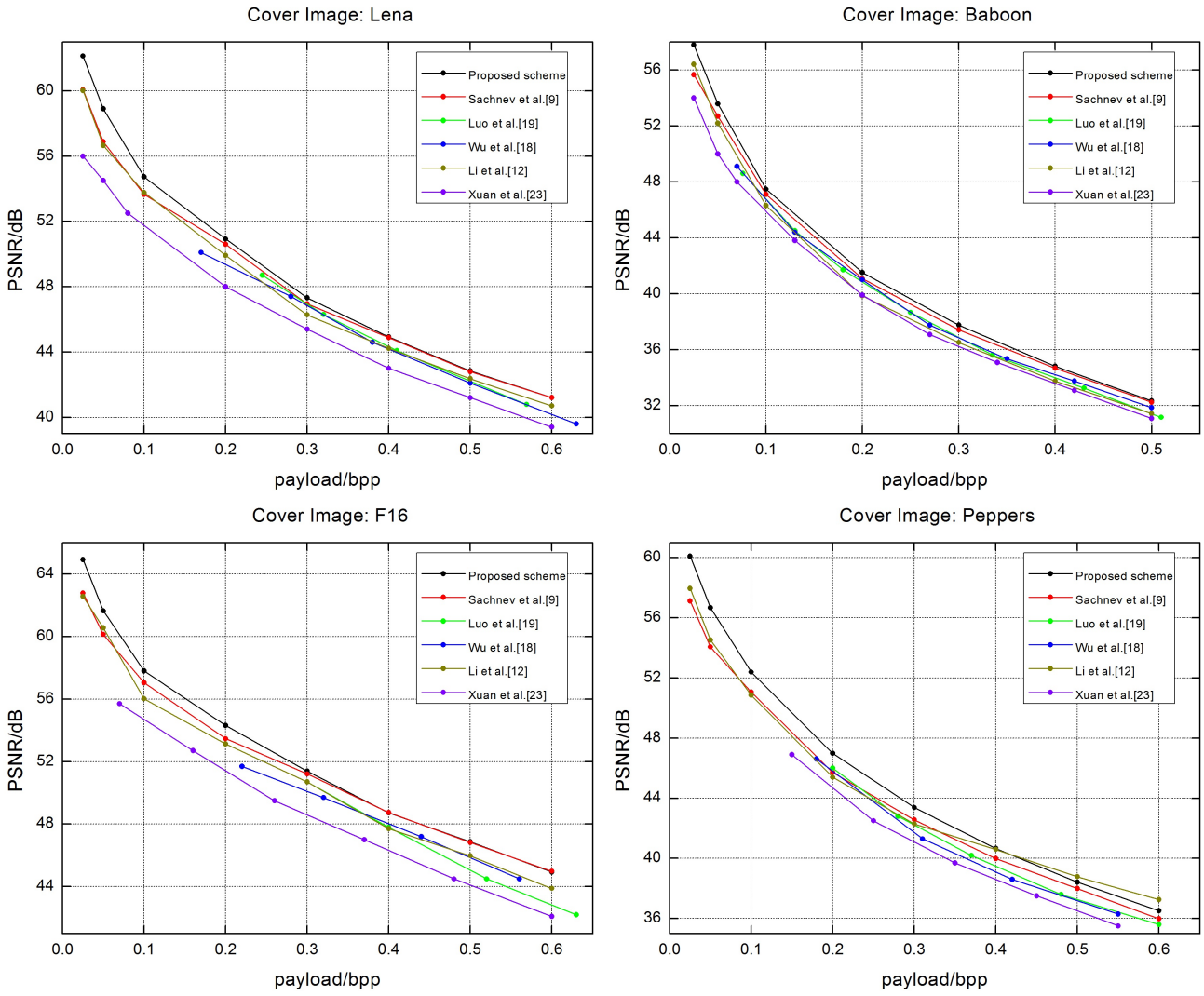

Fig. 8. Performance comparison between the proposed scheme and other related schemes

TABLE III
THE COMPARISON BETWEEN OUR PROPOSED SCHEME AND LI *et al*'S METHOD [21] FOR SMALL PAYLOAD

Test images	Algorithm	0.5×10^4bits (0.019bpp)	1.0×10^4bits (0.038bpp)	1.5×10^4bits (0.057bpp)	2.5×10^4bits (0.095bpp)
Lena	Li *et al*'s method [21] (dB)	63.119	59.703	57.684	55.149
	Proposed scheme (dB) Percentage (χ)	63.376 (30%)	60.089 (30%)	58.021 (40%)	55.212 (40%)
Baboon	Li *et al*'s method [21] (dB)	58.684	53.924	-	-
	Proposed scheme (dB) Percentage (χ)	59.066 (20%)	55.081 (30%)	52.289 (50%)	48.087 (50%)
F16	Li *et al*'s method [21] (dB)	66.587	63.161	60.940	57.923
	Proposed scheme (dB) Percentage (χ)	65.909 (10%)	62.959 (20%)	60.768 (30%)	57.945 (50%)
Peppers	Li *et al*'s method [21] (dB)	60.667	57.160	55.006	51.689
	Proposed scheme (dB) Percentage (χ)	61.487 (30%)	57.516 (40%)	55.929 (50%)	51.507 (50%)

than our scheme, which leads to a less sized location map. Consequently, Li *et al*'s method may outperform ours for some images with much more boundary pixels, such as Pepper, at high data payload.

For small data payload (ER$<$ 0.1bpp), we further compare the performance of our GA based scheme with the one of Li's method [21], which is summarized in Table III. Note that, for small data payload embedding, we take the top $\chi(\%)(\chi \in \Lambda_1)$

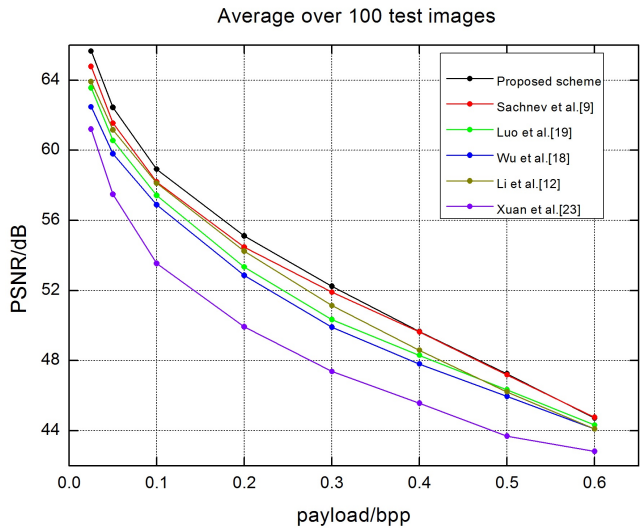

Fig. 9. Average performance comparison for 100 test images from Bossbase [27]

of the sorted prediction errors of both the Cross and Round sets as carrier images and the "-" in Table III denotes that there is no result reported for the corresponding bpp. It is observed that, although we only make use of a few fixed percentage χ in Λ_1, the performance of the proposed scheme is still slightly better than the one of Li's method, which is the state-of-the-art for small data payload embedding.

C. Practical evaluation of computational complexity

In this subsection, we further evaluate the practical computation cost in terms of computation time (CmpTime) of our GA based multiple reversible embedding scheme on different image sizes, and briefly analyze the practical computational complexity of our scheme and other involved schemes ([9], [12], [18], [19], [21] and [23]). Since any HS based embedding process needs to undergo three similar steps, i.e., generation of carrier images, peak and zero bin selection and reversible embedding, we only compare the CmpTime of peak and zero bin determination, which is the major difference between our scheme and others. For schemes [9], [12] and [21], since the peak and zero bins are fixedly selected, their CmpTimes are negligible. While the peak and zero bin pairs for schemes in [18], [19] and [23] are determined on the basis of some empirical rules, and their CmpTimes are also negligibly small.

In our simulation, we test the CmpTime of the proposed GA scheme in the Cross set of rhombus prediction with various image sizes for different payload, i.e., 0.2bpp, 0.3bpp and 0.6bpp. The simulation is implemented with Matlab on a 3.2 GHz Intel Pentium(R) Dual Core CPU with 4GB memory. And the parameter setting for GA as shown in Table I is also adopted in our experiment. In the interest of fair comparison, we randomly select 100 grayscale images of $512 \times 512 \times 8$ bits from Bossbase ver.1.01 [27], which are then subsequently processed by converting to images of $1024 \times 1024 \times 8$ bits and $2048 \times 2048 \times 8$ bits through interpolation. The average CmpTimes over 100 images for different payloads and 3 image resolutions with the proposed GA based scheme are summarized in Table IV. It is observed that: (1) the average CmpTime of the GA based scheme for 3 image resolutions is nearly the same, i.e., around 2.0 s, indicating that, with given initial histogram, the computational cost of our scheme is irrelevant to the cover image size; (2) our scheme could be implemented in a quite affordable computational cost.

TABLE IV
THE AVERAGE COMPUTATION TIME (CMPTIME) OF THE GA BASED OPTIMIZATION SCHEME

Test image size	Payload (bit per pixel)	CmpTime (second)
$512 \times 512 \times 8$	0.2bpp	1.783
	0.3bpp	1.838
	0.6bpp	1.913
$1024 \times 1024 \times 8$	0.2bpp	2.042
	0.3bpp	2.030
	0.6bpp	1.888
$2048 \times 2048 \times 8$	0.2bpp	2.482
	0.3bpp	2.253
	0.6bpp	2.241

VI. CONCLUSION

In this paper, an efficient GA based multiple embedding scheme is proposed for HS based reversible data hiding. By developing the rate and distortion model in terms of multiple pairs of peak and zero bins, the HS based multiple embedding is formulated as the problem of rate and distortion optimization. An evolutionary optimization algorithm, i.e., genetic algorithm (GA), is then employed to solve the optimization problem, which could not only adaptively determine the proper pair number of the peak and zero bins but also their corresponding nearly optimal values for HS based multiple embedding. Two main propositions in distortion computation are also obtained to facilitate the development of fast algorithm for distortion evaluation and the massive reduction of the solution space, which are preferable for practical application of GA. By partitioning the image into interleaved Cross and Round sets, the precise rhombus prediction and sorting are incorporated in the process of HS multiple embedding. Extensive simulations are carried out, which demonstrates the superior rate and distortion performance of the proposed scheme.

ACKNOWLEDGMENT

The authors would like to thank the anonymous reviewers and associate editor for their comments that greatly improved the manuscript.

REFERENCES

[1] M. Barni, F. Bartolini, I. J. Cox, J. Hernandez, and F. Perez-Gonzalez, "Digital watermarking for copyright protection: a. communications perspective," *Communications Magazine, IEEE*, vol. 39, no. 8, pp. 90–91, 2001.

[2] H. Tian, Y. Zhao, R. Ni, L. Qin, and X. Li, "Ldft-based watermarking resilient to local desynchronization attacks," *Cybernetics, IEEE Transactions on*, vol. 43, no. 6, pp. 2190–2201, Dec 2013.

[3] J. Barton, "Method and apparatus for embedding authentication information within digital data," Jul. 8 1997, US Patent 5,646,997.

[4] J. Fridrich, M. Goljan, and R. Du, "Invertible authentication," in *Proc. SPIE Photonics West*, vol. 3971, no. 2, 2001, pp. 197–208.

[5] M. U. Celik, G. Sharma, A. M. Tekalp, and E. Saber, "Lossless generalized-lsb data embedding," *Image Processing, IEEE Transactions on*, vol. 14, no. 2, pp. 253–266, 2005.

[6] J. Tian, "Reversible data embedding using a difference expansion," *IEEE Trans. Circuits Syst. Video Techn.*, vol. 13, no. 8, pp. 890–896, 2003.

[7] L. Kamstra and H. J. Heijmans, "Reversible data embedding into images using wavelet techniques and sorting," *Image Processing, IEEE Transactions on*, vol. 14, no. 12, pp. 2082–2090, 2005.

[8] D. M. Thodi and J. J. Rodríguez, "Expansion embedding techniques for reversible watermarking," *Image Processing, IEEE Transactions on*, vol. 16, no. 3, pp. 721–730, 2007.

[9] V. Sachnev, H. J. Kim, J. Nam, S. Suresh, and Y. Q. Shi, "Reversible watermarking algorithm using sorting and prediction," *Circuits and Systems for Video Technology, IEEE Transactions on*, vol. 19, no. 7, pp. 989–999, 2009.

[10] Y. Hu, H.-K. Lee, and J. Li, "De-based reversible data hiding with improved overflow location map," *Circuits and Systems for Video Technology, IEEE Transactions on*, vol. 19, no. 2, pp. 250–260, 2009.

[11] D. Coltuc, "Improved embedding for prediction-based reversible watermarking," *Information Forensics and Security, IEEE Transactions on*, vol. 6, no. 3, pp. 873–882, 2011.

[12] X. Li, B. Yang, and T. Zeng, "Efficient reversible watermarking based on adaptive prediction-error expansion and pixel selection," *Image Processing, IEEE Transactions on*, vol. 20, no. 12, pp. 3524–3533, 2011.

[13] Z. Ni, Y.-Q. Shi, N. Ansari, and W. Su, "Reversible data hiding," *Circuits and Systems for Video Technology, IEEE Transactions on*, vol. 16, no. 3, pp. 354–362, 2006.

[14] G. Xuan, Q. Yao, C. Yang, J. Gao, P. Chai, Y. Q. Shi, and Z. Ni, "Lossless data hiding using histogram shifting method based on integer wavelets," in *Digital Watermarking*. Springer, 2006, pp. 323–332.

[15] C.-C. Lin, W.-L. Tai, and C.-C. Chang, "Multilevel reversible data hiding based on histogram modification of difference images," *Pattern Recognition*, vol. 41, no. 12, pp. 3582–3591, 2008.

[16] W.-L. Tai, C.-M. Yeh, and C.-C. Chang, "Reversible data hiding based on histogram modification of pixel differences," *Circuits and Systems for Video Technology, IEEE Transactions on*, vol. 19, no. 6, pp. 906–910, 2009.

[17] D.-G. Yeo, H.-Y. Lee, and B. M. Kim, "High capacity reversible watermarking using differential histogram shifting and predicted error compensation," *Journal of Electronic Imaging*, vol. 20, no. 1, pp. 013 001–013 001, 2011.

[18] H.-T. Wu and J. Huang, "Reversible image watermarking on prediction errors by efficient histogram modification," *Signal Processing*, vol. 92, no. 12, pp. 3000–3009, 2012.

[19] L. Luo, Z. Chen, M. Chen, X. Zeng, and Z. Xiong, "Reversible image watermarking using interpolation technique," *Information Forensics and Security, IEEE Transactions on*, vol. 5, no. 1, pp. 187–193, 2010.

[20] X. Gao, L. An, Y. Yuan, D. Tao, and X. Li, "Lossless data embedding using generalized statistical quantity histogram," *Circuits and Systems for Video Technology, IEEE Transactions on*, vol. 21, no. 8, pp. 1061–1070, 2011.

[21] X. Li, W. Zhang, X. Gui, and B. Yang, "A novel reversible data hiding scheme based on two-dimensional difference-histogram modification," *Information Forensics and Security, IEEE Transactions on*, vol. 8, no. 7, pp. 1091–1100, 2013.

[22] B. Yang, M. Schmucker, C. Busch, X. Niu, and S. Sun, "Approaching optimal value expansion for reversible watermarking," in *Proceedings of the 7th workshop on Multimedia and security*. ACM, 2005, pp. 95–102.

[23] G. Xuan, Y. Q. Shi, P. Chai, J. Teng, Z. Ni, and X. Tong, "Optimum histogram pair based image lossless data embedding," in *Transactions on Data Hiding and Multimedia Security IV*. Springer, 2009, pp. 84–102.

[24] Y.-T. Wu and F. Y. Shih, "Genetic algorithm based methodology for breaking the steganalytic systems," *Systems, Man, and Cybernetics, Part B: Cybernetics, IEEE Transactions on*, vol. 36, no. 1, pp. 24–31, 2006.

[25] D. E. Goldberg, *Genetic Algorithms in Search, Optimization and Machine Learning*, 1st ed. Boston, MA, USA: Addison-Wesley Longman Publishing Co., Inc., 1989.

[26] [Online]. Available: http://sipi.usc.edu/database/

[27] P. Bas, T. Filler, and T. Pevnỳ, " break our steganographic system: The ins and outs of organizing boss," in *Information Hiding*. Springer, 2011, pp. 59–70. [Online]. Available: http://www.agents.cz/boss/

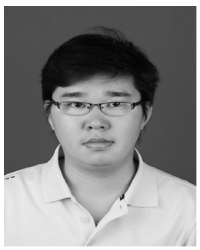

Junxiang Wang received the M.S. and Ph.D. degrees from the Harbin Institute of Technology and Sun Yat-Sen University in 2008 and 2012, respectively. He is currently an Associate Professor with the School of Mechanical and Electronic Engineering, Jingdezhen Ceramic Institute (JCI), Jiangxi, China. His research interests include information security and image processing.

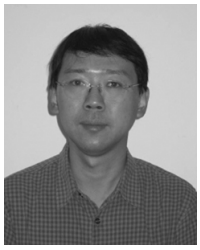

Jiangqun Ni (M'12) received the Ph.D. degree in electronic engineering from the University of Hong Kong, Hong Kong, in 1998. He worked as a Postdoctoral Fellow for a joint program between the Sun Yat-sen University and the Guangdong Institute of Telecommunication Research during 1998 through 2000. Since 2001, he has been with the school of Information Science and Technology, Sun Yat-sen University, Guangzhou, China, where he is currently a Professor. His research interests include data hiding and digital image forensics, image-based modeling and rendering, and image/video processing. He has published more than 50 papers in these areas.

Xing Zhang received the B.S. degree in Communication Engineering from Sun Yat-Sen University, Guangzhou, China, in 2013. He is currently pursuing the M.S. degree with the School of Information Science and Technology, Sun Yat-Sen University, Guangzhou, China. His current research interests include digital watermarking and image processing.

Yun-Qing Shi (M'88-SM'92-F'05) has joined New Jersey Institute of Technology, USA, since 1987. He obtained his M.S. degree from Shanghai Jiao Tong University, China; his Ph.D. degree from University of Pittsburgh, USA. His research interests include digital data hiding, forensics and information assurance, visual signal processing and communications. He is an author/coauthor of 300 papers, one book, five book chapters, and an editor of 10 books. He holds 28 US patents. He obtained Innovators Award 2010 by New Jersey Inventors Hall of Fame for Innovations in Digital Forensics and Security. His US patent 7,457,341 entitled "System and Method for Robust Reversible Data Hiding and Data Recovery in the Spatial Domain" won 2010 Thomas Alva Edison Patent Award by Research and Development Council of New Jersey. He served as an associate editor of IEEE Transactions on Signal Processing and IEEE Transactions on Circuits and Systems (II), and a few other journals; also served as the technical program chair of IEEE ICME07, co-technical chair of IWDW06, 07, 09, 10, 11, 12, 13 and IEEE MMSP05, co-general chair of IEEE MMSP02, a Distinguished Lecturer of IEEE CASS. He is a member of a few IEEE technical committees, and a Fellow of IEEE since 2005.